Applied Thermal Engineering 260 (2025) 124952

Contents lists available at ScienceDirect

Applied Thermal Engineering

journal homepage: www.elsevier.com/locate/apthermeng

Research Paper

Techno-economic assessment of a Carnot battery thermally integrated with a data center

Chiara Poletto [a,*], Andrea De Pascale [a], Saverio Ottaviano [a], Olivier Dumont [b], Lisa Branchini [a]

[a] University of Bologna, Viale del Risorgimento 2, 40136 Bologna, Italy
[b] University of Liège, Allée de la Découverte 17, 4000 Liège, Belgium

ARTICLE INFO

Keywords:
Carnot battery
Data center
Waste heat recovery
Heat pump
Organic Rankine cycle
Energy management

ABSTRACT

Carnot batteries (CBs) are gaining interest as energy storage solutions, particularly when waste heat is available for thermal integration. Data centers (DCs) represent a relevant source of waste heat, as they convert most of the supplied electricity into low-grade heat, and their utilization is expected to continue increasing in the future. This study explores the feasibility of integrating an Organic Rankine Cycle (ORC)/Heat Pump (HP) CB with a DC powered by a photovoltaic power plant. First, from the thermodynamic analysis conducted in design conditions, the hydrofluoroolefin R1233zd(E) results in the most suitable working fluid, leading to 43 % roundtrip efficiency. Then, a detailed semi-empirical off-design model of a CB is employed in a rule-based control strategy to handle the ORC/HP operations. If the HP is thermally integrated with the DC waste heat, a higher coefficient of performance is achieved, and the consumption of the DC cooling system is reduced. A sensitivity analysis is conducted to explore the impact of the storage volume and the energy prices on the integrated system's techno-economic performance. The CB implementation is economically feasible when the electricity price is high, reaching a yearly gain of 7744 €, and a simple payback period of 10 years when considering a DC electric consumption of 200 kWe and a 25 kWe-sized HP/ORC. The gain increases if the electric surplus cannot be sold, obtaining a 4-year payback period. Eventually, we perform a comparison with an ORC-only configuration to assess the CB's technical and economic convenience.

1. Introduction

The strong development of the information and communication technology (IT) field, which occurred during the last few decades, has brought a rapid spread of data centers (DCs) as key infrastructures for services provided via the Internet. Today, the world's total electricity consumption is attributable to 2 % to DCs, due to the strong development of the IT sector [1], and this contribution is expected to increase, in view of the continuous growth of the IT field [2]. Since almost the whole of DC servers' electricity demand is converted to thermal energy [3], a significant amount of energy is required for cooling. It is required to ensure that server equipment temperatures do not excessively increase to cause system performance degradation and irreversible damage. As a result, usually 35-40 % of the total energy in a DC is spent for cooling [4], and a significant portion of energy is dissipated as waste heat to the ambient.

In light of the above, DCs are well suited for coupling with thermal energy recovery technologies, like organic Rankine cycle (ORC) power plants, systems that are location-independent and easily scalable in capacity [5]. The main drawback associated with DC waste heat recovery by ORC technology is the very low temperature, less than 60 °C [6], at which the heat is typically released. For this reason, almost all the few works investigating this application, integrate the ORC with other technologies, especially heat pumps (HPs). Ebrahimi et al. [7], proposed the integration of an ORC system into a DC cooling system, while Jawad Al-Tameemi [8] integrated an ORC, a HP and a gas burner to provide cooling for the DC as well as supply hot water for central heating. Temiz and Dincer [9] proposed an integrated system, which includes a parabolic trough-type concentrated solar plant with a Rankine cycle, a bifacial photovoltaic plant, a hydrogen storage system, and a Li-Br absorption refrigeration cycle. Marshall and Duquette [5], instead, analysed an ORC system assisted by a HP integrated with the cooling system.

An alternative solution to recover and utilize DC waste heat is to address the released thermal energy to help satisfy residential users' heat demand. Jang et al. [10] proposed a novel waste heat recovery water-source HP system to reduce energy consumption, by recovering

* Corresponding author.
E-mail address: chiara.poletto3@unibo.it (C. Poletto).

https://doi.org/10.1016/j.applthermaleng.2024.124952
Received 31 January 2024; Received in revised form 21 May 2024; Accepted 13 November 2024
Available online 16 November 2024

Nomenclature

Symbols

C	cost (€)
COP	coefficient of performance (−)
DPB	discounted payback period (year)
E	electric energy (kWh)
ERE	energy reuse effectiveness (−)
G	irradiance (W/m^2)
GWP	global warming potential (−)
h	enthalpy (kJ/kg)
I	investment cost (€/kW)
$\dot{m}$	mass flow rate (kg/s)
ODP	ozone depletion potential (−)
p	pressure (bar)
P	power (kW)
PUE	power usage effectiveness (−)
Q	thermal energy (kWh)
$\dot{Q}$	thermal power (kW)
r	discounted rate (−)
s	entropy (kJ/(kg K))
SC	subcooling degree (K)
SH	superheating degree (K)
SPB	simple payback period (year)
T	temperature (°C)
TC	cold side temperature (°C)
TH	hot side temperature (°C)
UF	utilization factor (%)
x	quality (−)

Greek

β	temperature coefficient (%/°C)
γ	irradiance coefficient (% m^2/W)
Δ	difference (−)
η	efficiency (%)

Subscripts

amb	ambient
ave	average
chiller	chiller
comp	compressor
cooling	cooling system
dem	demand
el	electric
em	electromechanical
exp	expander
fans	fans
glide	temperature glide
is	isentropic
in	inlet
k	condensation
light&loss	other losses included lighting
max	maximum
min	minimum
noCB	without Carnot battery
NOCT	nominal operating cell
out	outlet
pp	pinch point
pump	pump
Q	thermal energy
ref	reference
reuse	recovered energy
rt	roundtrip
sink	thermal sink
source	thermal source
th	thermodynamic
TH	thermal user
v	evaporation
wf	working fluid
year	year

Acronyms

CB	Carnot battery
DC	data center
HP	heat pump
IT	information technology equipment
ORC	organic Rankine cycle
PV	photovoltaic
sfC	cold secondary fluid
sfH	hot secondary fluid
TES	thermal energy storage

waste heat from the DC. Hou et al. [11] investigated the optimal control of the DC waste heat-based heat prosumer utilizing a model predictive control scheme. They introduced a short-term water tank thermal energy storage (TES), which allows an increase in the flexibility of the thermal energy usage. More in general, Liu et al. [12] provided an extensive overview of TES technologies integrated with cooling systems to achieve energy and cost savings if applied to DCs.

Based on the above literature review, it is interesting to investigate the integration of a Carnot battery (CB) in DC cooling systems. CBs belong to grid-scale electricity storage technologies and represent a solution to limit the mismatch between renewable energy source production and electricity demand [13]. This solution has been proposed by Dumont [14]. The CB working principle is based on storing electric energy in surplus in the form of thermal energy: in the charging phase, the electric surplus is used as input to let thermal energy flow against a thermal gradient, from a lower temperature heat sink to a higher temperature heat reservoir; in the discharging phase, the high-temperature reservoir is discharged to power a heat engine, which produces mechanical work (then converted into electric energy). The main technologies adopted to operate the charging/discharging phases are based on the direct and inverse Rankine cycle, and the direct and inverse Brayton cycle [15]. Furthermore, CBs show higher performance when integrated into waste heat recovery systems because the increase of very low-grade waste heat enthalpy content allows to reduce the temperature lift in the charging phase, increasing the inverse cycle performance, without reducing the discharging conversion efficiency [16]. In this context, to the Authors' best knowledge, the application of CB technology to DCs is investigated only by Laterre et al. [17]. Their research assesses the potential of integrating an electric booster-assisted CB in DCs to enhance electrical storage efficiency through waste heat recovery. The study explores various scenarios and climatic conditions using multi-criteria optimization and a thermodynamic model. Findings indicate extended payback periods, but reducing CB capital costs could expedite economic returns. The choice between HPs and resistive heaters depends on heat source temperatures. The study identifies an efficiency/charging capacity trade-off, suggesting a need for efficient booster configurations to improve the techno-economic performance of thermally integrated CB systems. Laterre et al. provide several recommendations for future research and developments, faced in our study, such as i) investigating more efficient configurations for the system during the charging phase, ii) addressing flexibility constraints and part-load operations, iii) reducing CB capital costs by adopting reversible

HP/ORC systems and a single stratified tank as TES, iv) including additional revenue streams in the integrated system.

1.1. Contribution of this study

In light of the above, this study aims to fill some of the gaps highlighted by Laterre et al. [17], investigating the feasibility of integrating a reversible HP/ORC Carnot battery in the cooling system of a DC fed by a photovoltaic (PV) power plant. Being one of the first attempts to apply the CB technology to the DC context, this study offers a novel approach to address the challenges of waste heat recovery and electrical storage efficiency enhancement in a critical energy-consuming sector, in which heat is currently completely wasted. The first part of the work is dedicated to the overall design of the proposed plant, including the selection of the most suitable working fluid for the HP and ORC. After a first thermodynamic screening of well-proven working fluids in HP and ORC applications, the most promising working fluid for DC application is detected by performing a sensitivity analysis through constant-efficiency models of HP and ORC. These models are subsequently adopted, with the selected working fluid, to design the CB and the PV size suitable for the considered application. Based on the overall design provided at the first stage, a detailed semi-empirical model of a reversible HP/ORC and a stratified TES model are used to simulate the operation of the CB in off-design conditions. A rule-based management strategy for the optimal CB operation is developed, aimed to maximize the economic gain obtainable in a year of operation. The DC waste heat is partially recovered through the HP when the PV production overcomes the DC demand, and it is stored at a higher temperature in a sensible TES. When the PV production becomes lower than the DC electric demand, the stored thermal energy is used to power the ORC, reducing the electricity that must be purchased from the grid. Furthermore, the possibility of directing the high-temperature thermal energy to a thermal user in wintertime is included as an additional revenue stream. Thus, the CB integration with the DC cooling system provides a double advantage. On the one hand, the thermal energy released by the servers is not dissipated to the environment, increasing its quality with the HP. It is used either to produce electricity with the ORC for on-site consumption (in case of renewable electric energy deficit) or to supply a user's thermal demand. On the other hand, the proposed system reduces the cooling load provided by the DC cooling system, i.e., the corresponding electricity consumption, because the HP cold source partially replaces the original cooling system of the DC. Therefore, unlike previous studies, this work adopts a comprehensive approach to the design and optimization of the proposed integrated system, encompassing the selection of optimal working fluids for the HP and ORC, the sizing of the CB and PV components, and the development of a rule-based management strategy for maximizing the economic gain. The integration of multiple revenue streams is explored using un-exploited low-temperature heat and PV electrical surplus to produce high-temperature heat. The double possibility of using the high-temperature heat to satisfy the DC electric demand (through the ORC, in case of PV deficit) or to direct it to a thermal user would increase efficiency and revenues of proposed solution. Two different electricity and thermal energy price scenarios are investigated and compared. Moreover, the proposed configuration is compared with the simpler solution consisting of a sole ORC with the same size and characteristics, recovering the waste heat from the DC. Such a comparative analysis provides a comprehensive evaluation of the advantages and limitations of different waste heat recovery approaches in DC environments.

2. Materials and methods

In this section, the analysed system is described, the working fluid selection and a preliminary thermodynamic investigation are performed, the size of the CB is determined, the control strategy is presented, and the ORC-only case is introduced. Hypothesis, boundary conditions, and key performance indicators are defined.

2.1. The integrated system configuration

The integration of a reversible HP/ORC CB with a sensible TES in the cooling system of a DC, the main components and their function, and the energy flows are described below, according to the numbers in Fig. 1:

1. An on-site DC server, which requires electric power demand, assumed constant over time.
2. The DC cooling system (relying on direct air cooling and water cooling through a chiller), which prevents the temperature from increasing above the IT temperature limits.
3. An on-site solar PV power plant, which can feed the DC and its cooling system electric demand. Its production depends on actual solar irradiance, and it can be higher or lower than the electric demand.
4. The electric grid, which provides the flexibility to cover the DC and the cooling system demanded electricity when the integrated system production is lower, and to absorb the exceeding electricity produced by the PV power plant. The electric grid prevents the fluctuation and intermittency of PV production from affecting the stable operation of the DC.
5. The HP/ORC CB, which is charged (HP mode) by utilizing surplus energy from the PV power plant and waste heat from the DC, and discharged to return the stored energy in the form of electricity (ORC mode) and to directly provide thermal energy (thermal discharge) from the storage tank to a thermal user. The DC waste heat is recovered bypassing part of the hot water directed to the chiller into the HP evaporator. In this way, part of the cooling load is absorbed by the HP, instead of the cooling system.
6. A high-temperature thermal user (e.g., a district heating substation), which can absorb the thermal energy whole surplus produced by the HP that is not stored in the TES, reducing the thermal consumption of conventional heat production systems already existing.
7. The ambient, at the outside air temperature, which operates as a cold sink for the DC cooling system and the ORC unit.

2.2. Preliminary thermodynamic investigation on heat pump and organic Rankine cycle

To optimally design the CB components and to identify the most suitable fluid for the considered application, a systematic comparison is performed in terms of thermodynamic performance. A set of fluids is selected, among the fluids available in CoolProp library [18], with a critical temperature slightly higher than the temperature levels of the DC application, and with low environmental impact. The CB thermodynamic performance, in terms of HP coefficient of performance, ORC efficiency, and roundtrip efficiency are calculated and compared through a lumped-parameters thermodynamic model. The model simulates a simple HP cycle and a simple ORC configuration, both working in subcritical conditions and requiring the minimum number of main components. The HP and ORC thermodynamic cycles are shown in Fig. 2 using R1233zd(E) as the working fluid.

The developed calculation routine, implemented in MATLAB environment, determines, for a given operating fluid, the evaporation pressure (p_v) and the condensation pressure (p_k), using as input values: cold source and hot source temperature at the inlet (TC_{in}, TH_{in}), the glide terms (sfC_{glide}, sfH_{glide}), and the pinch point temperature difference (ΔT_{pp}). The equations and the assumptions adopted to model the HP cycle and the ORC are listed in Table 1. Constant isentropic efficiency for the compression (in both modes) and the expansion (in ORC mode), isenthalpic expansion (in HP mode), isobaric evaporation and condensation (in both modes) and negligible pressure losses in the heat exchangers are assumed. The thermodynamic properties of the

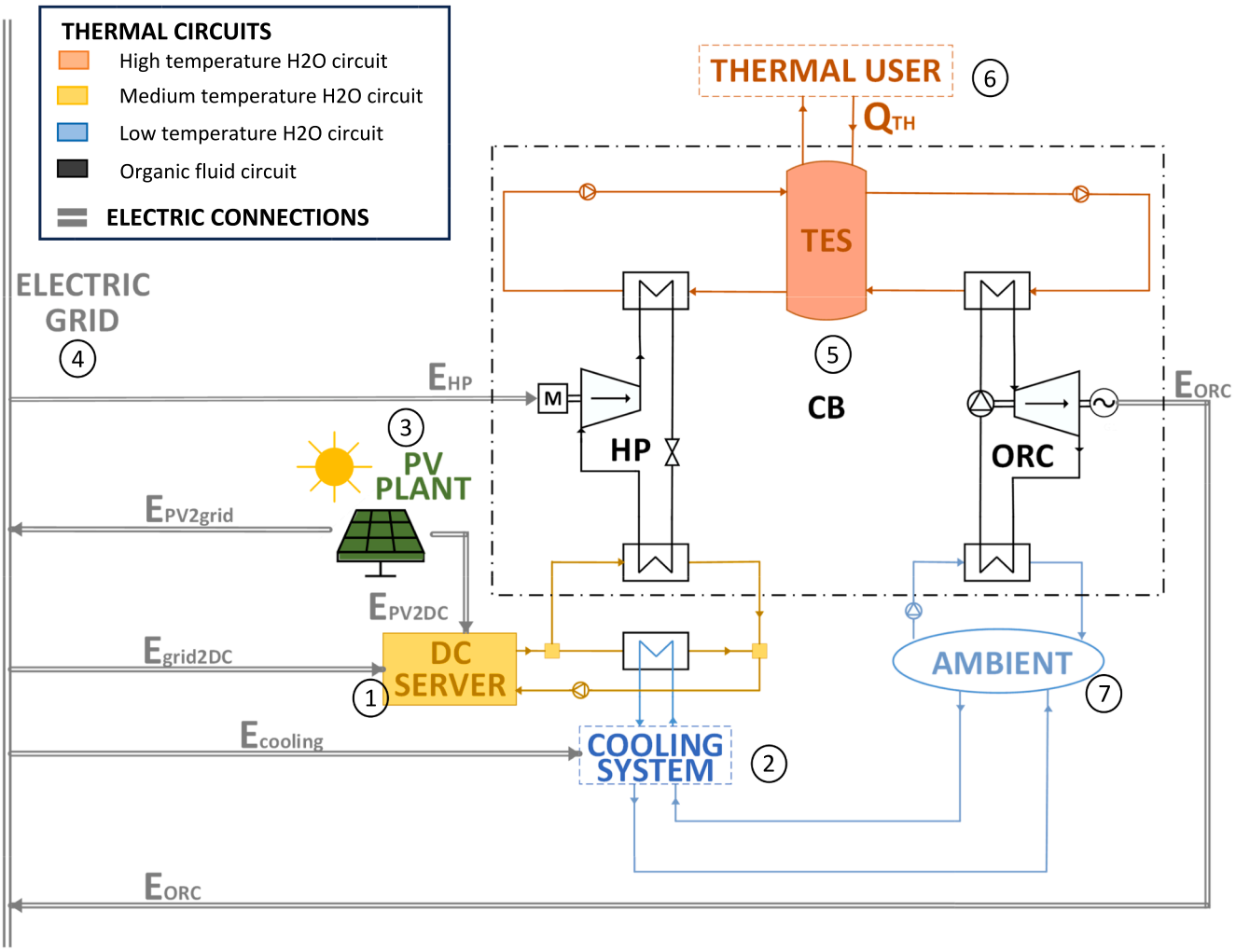

Fig. 1. Integrated system configuration layout, where the main components, the thermal circuits, and the electric connections are shown.

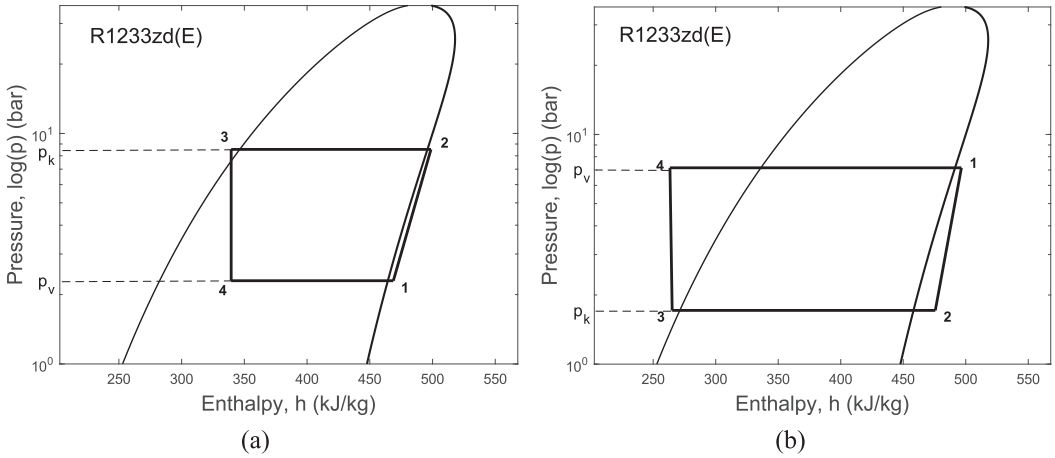

Fig. 2. Pressure-enthalpy diagrams showing the (a) HP cycle and (b) ORC, in case of R1233zd(E).

investigated fluids are obtained through CoolProp database [18]. The HP performance is evaluated through the thermodynamic coefficient of performance (COP_{th} in Eq. (11)), defined as the ratio between the produced specific thermal energy and the specific work absorbed in the compression process. The ORC efficiency performance is evaluated through the net thermodynamic efficiency ($\eta_{ORC,th}$ in Eq. (22)), defined as the ratio between the cycle output net specific work (the specific work produced during the expansion process reduced by the specific work required for liquid compression) and the cycle specific thermal energy input.

In order to design the CB for a given HP input electric power ($P_{el,HP}$), it is possible to calculate the working fluid flow rate ($\dot{m}_{wf}$) by assuming

Table 1
Equations used to model the HP and ORC thermodynamic performance.

HP mode		
Secondary fluids	$TC_{out} = TC_{in} - sfC_{glide}$	(1)
	$TH_{out} = TH_{in} + sfH_{glide}$	(2)
Pressures	$p_v = p(TC_{out} - \Delta T_{pp}, x = 1)$	(3)
	$p_k = p(TH_{out} + \Delta T_{pp}, x = 0)$	(4)
State point 1	$h_1 = h(p_v, TC_{out} - \Delta T_{app} + SH)$	(5)
	$s_1 = h(p_v, h_1)$	(6)
State point 2	$h_{2,is} = h(p_k, s_1)$	(7)
	$h_2 = h_1 + (h_{2,is} - h_1)/\eta_{is,comp}$	(8)
State point 3	$h_3 = h(p_k, TH_{out} + \Delta T_{pp} + SC)$	(9)
State point 4	$h_4 = h_3$	(10)
Thermodynamic COP	$COP_{th} = (h_2 - h_3)/(h_2 - h_1)$	(11)
ORC mode		
Secondary fluids	$TH_{out} = TH_{in} - sfH_{glide}$	(12)
	$TC_{out} = TC_{in} + sfC_{glide}$	(13)
Pressures	$p_v = p(TH_{out} - \Delta T_{pp}, x = 1)$	(14)
	$p_k = p(TC_{out} + \Delta T_{pp}, x = 0)$	(15)
State point 1	$h_1 = h(p_v, TH_{out} - \Delta T_{pp} + SH)$	(16)
	$s_1 = h(p_v, h_1)$	(6)
State point 2	$h_{2,is} = h(p_k, s_1)$	(7)
	$h_2 = h_1 - \eta_{is,exp}(h_1 - h_{2,is})$	(17)
State point 3	$h_3 = h(p_k, TC_{out} + \Delta T_{pp} - SC)$	(18)
	$s_3 = h(p_k, h_3)$	(19)
State point 4	$h_{4,is} = h(p_v, s_3)$	(20)
	$h_4 = h_3 + (h_{4,is} - h_3)/\eta_{is,pump}$	(21)
Net thermodynamic efficiency	$\eta_{ORC,th} = [(h_1 - h_2) - (h_4 - h_3)]/(h_1 - h_4)$	(22)

an electromechanical conversion efficiency (η_{em}), and then evaluate the thermal power absorbed in the evaporator ($\dot{Q}_{source,HP}$) and released in the condenser ($\dot{Q}_{sink,HP}$), according to the following equations:

$$\dot{m}_{wf} = P_{el,HP} \bullet \eta_{em}/(h_2 - h_1) \tag{23}$$

$$\dot{Q}_{source,HP} = \dot{m}_{wf} \bullet (h_1 - h_4) \tag{24}$$

$$\dot{Q}_{sink,HP} = \dot{m}_{wf} \bullet (h_2 - h_3) \tag{25}$$

Since the HP source, in the considered application, matches the waste heat released by the DC, the reversible HP/ORC has been designed by choosing the size that allows to maximize the exploitation of DC discharged waste heat. In other words, $\dot{Q}_{source,HP}$ is calculated for different values of $P_{el,HP}$, and it is compared with the thermal power released by the DC.

2.3. The Carnot battery management description

Once the CB design is performed, the integrated system requires the implementation of an efficient scheduling strategy to manage the CB operation.

The control algorithm, implemented to solve the problem, is developed according to a rule-based strategy (Fig. 3). The algorithm determines when to activate/deactivate the CB and to switch its mode (HP/ORC), starting with an initial solution attempt and in accordance with the boundary conditions (i.e., PV electric production, DC electric demand, weather conditions, electricity price). An economic-objective function is used to manage the CB scheduling. The objective function (Eq. (26)) is the economic gain (ΔC) between the two configurations with and without the CB intervention in the integrated system.

$$\Delta C = E_{ORC} \bullet C_{el} + \Delta E_{cooling} \bullet C_{el} + Q_{TH} \bullet C_Q - E_{HP} \bullet C_{el} \tag{26}$$

In particular, the gain, assessed and maximized at each time step, is the sum of three positive terms and a negative term. The first two contributions are proportional to respectively the energy produced by the ORC (E_{ORC}), and the electric energy savings from the cooling system ($\Delta E_{cooling}$) achieved by utilizing the HP to remove DC waste heat. These terms are multiplied by the electricity price (C_{el}). The third term is due to the sale of thermal energy to the thermal user (Q_{TH}) and it is proportional to the thermal energy price (C_Q). The negative contribution is due to the renewable energy surplus which is used to power the HP (E_H), instead of being sold to the grid. The outcomes of the procedure are the HP/ORC energy values (all accounting for auxiliaries and loss contributions, including the ORC pump consumption) outlined in Eq. (26), which assesses the economic advantage of the CB integration.

The algorithm first computes the availability of renewable electric power, compared to the DC electricity demand. When the PV production cannot provide the DC electric demand (PV deficit), the algorithm examines the current electricity price (C_{el}). If it exceeds the average electricity price of the current day, and the temperature in the TES is above the ORC minimum operating temperature, then the ORC is activated, discharging the storage. When the PV production rises above the electric demand (PV surplus), the HP is activated to store the electric surplus in the form of thermal energy in the TES. If the HP is not allowed to work (because the storage is already full or the available electricity is not enough to run the HP above the technical minimum), the algorithm evaluates the economic feasibility of operating the ORC to generate a power surplus for sale to the grid. The option of allowing the HP to operate in power deficit, drawing electricity from the grid when prices are low, is not considered for the sake of a conservative approach.

Subsequently, the energy balance on the storage yields updated storage conditions in terms of temperature (T_{TES}) and thermal energy (Q_{TES}) availability. Additionally, it is assumed that, during the winter season, any excess thermal energy in the storage at temperatures exceeding $T_{TH,min}$, can be sold to an external thermal user (e.g., a district heating substation). This results in a thermal discharge, and the storage conditions are revised accordingly. The main rules to activate/deactivate the CB and to switch its mode, are summarized in Table 2.

Although the algorithm initially assesses the option of activating the ORC and subsequently considers the possibility of the thermal discharge, the implicit priority is given to the thermal discharge. Specifically, in the event of a surplus in renewable production, the HP is activated to charge the storage. Subsequently, two distinct scenarios unfold depending on the season. In wintertime, once the storage reaches a temperature value of $T_{TH,min}$, the HP production is addressed to the thermal user. In this way, as long as there is a surplus of renewable production, the HP continues operating to reduce the DC cooling load. In summertime, the HP operates until the storage is full ($T_{TES} < T_{TES,max}$). The storage is then discharged through the ORC when it becomes economically viable in terms of electricity prices. After the discharge phase, the HP resumes charging the storage, thereby reducing the DC cooling load. In case of a power deficit, the storage can be discharged through the ORC to generate electricity to meet the surplus demand of the DC. Notably, this situation predominantly occurs in summer when the storage can be maintained at full charge through HP operation. Conversely, in wintertime, HP production is promptly directed to the thermal user upon release into the TES, and the storage is not kept at full charge for ORC operation.

2.4. Off-design modelling of heat pump/organic Rankine cycle and storage within the CB

The HP/ORC system [19] is modelled following a semi-empirical method presented in [20], rescaled and validated using, as a reference, the CB prototype installed at the University of Liège [21]. More in detail, the heat exchangers are simulated according to the moving boundaries method [22]. Cooper's, Gnielinski's and Dittus-Boelter's correlations are applied to assess evaporative, condensing and single-phase convective heat transfer coefficients. The scroll compressor/expander is modelled using Lemort's lumped-parameters approach [23], accounting for under and overexpansion/compression losses, pressure drops, heat transfers at inlet/outlet ports, internal leakages, mechanical losses, and heat losses. The ORC pump is modelled, following the

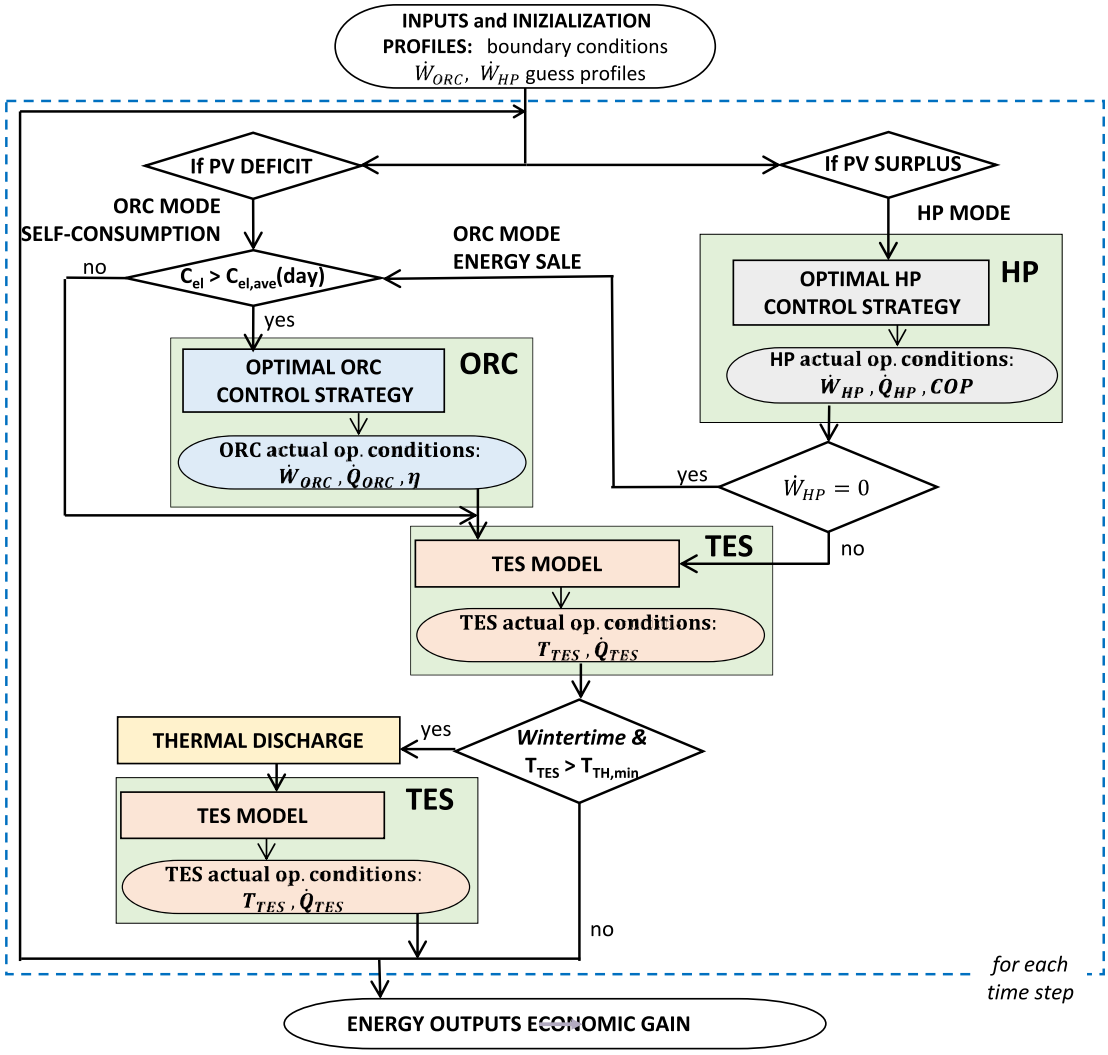

Fig. 3. Carnot Battery management flowchart.

Table 2
List of the main rules for each mode activation

Mode	Rule
Th. Charge (HP mode)	HP is activated only in case of:PV surplus ($P_{el,PV} > P_{el,dem}$) &$T_{TES} < T_{TES,max}$
Th. Discharge	In wintertime, priority of heat from TES to TH user when $T_{TES} > T_{TH,min}$
El. Discharge (ORC mode)	ORC is activated in case of:PV deficit ($P_{el,PV} < P_{el,dem}$) & $T_{TES} > T_{ORC,min}$ &$C_{el} > C_{el,ave}(day)$ *OR* if:PV surplus ($P_{el,PV} > P_{el,dem}$) & HP off (due to full TES or low PV surplus) &$C_{el} > C_{el,ave}(day)$

approach described in [24], through a lumped-parameters equation, considering rotational speed, volume flow rate, pressure rise, and deviations from nominal points. The expansion valve is modelled as an isenthalpic expansion between maximum and minimum cycle pressures. The pressure drops are included, as well as auxiliary pumps consumption [25]. Lookup tables, obtained with the reversible HP/ORC model by simulating the system in a wide range of operating conditions, are used to speed up the Carnot battery management strategy. They represent the HP/ORC performance maps in design and off-design operation, and they allow the identification of the maximum efficiency operation under imposed boundary conditions. Considering the temperature of the cold source/sink, the available temperature in the storage, and the electric power availability/demand, the interpolation of the lookup tables provides the HP/ORC operating conditions that maximize the coefficient of performance (COP)/efficiency within operating constraints. The outputs of the lookup tables are: secondary fluids glides, working fluid flow rate, COP/efficiency, and actually produced/consumed power [25]. The lookup tables are built including the system's physical constraints and all the loss contributions (HP compressor, ORC pump, and auxiliary pumps).

The sensible TES is modelled as a one-dimensional vertical axis cylindrical stratified water tank, as presented in [26]. The storage volume is vertically discretized into equal layers, in which all the thermodynamic properties are considered constant. Therefore, the temperature and all the dependent properties vary only along the vertical direction between one layer and the other. The layers exchange thermal energy with the neighbours through convection and diffusion (representing the mixing of the water inside the tank and the temperature difference between neighbour layers), and with the external environment through wall conduction (representing the heat loss contribution, since the tank is not considered completely insulated – adiabatic – but with an efficiency between charging and discharging lower than 1). Energy conservation equation is applied to each tank's layer, deriving a system of ordinary differential equations [27], and solved numerically by adopting the upwind scheme [28]. The temperature profile in the tank is then provided as a function of time [26].

2.5. Orc-only configuration

An alternative solution to the CB integration for improving the DC energy efficiency consists of the direct recovery of the waste heat to power an ORC, which produces electric energy contributing to the DC electricity supply (Fig. 4). In this case, the ORC is connected to a heat source (DC waste heat) constantly available at the same temperature. However, when the ambient temperature (representing the cold sink) is too high, the ORC is switched off. The same performance maps describing the ORC operation adopted in the CB management strategy are used to evaluate the ORC performance in the ORC-only configuration.

2.6. Assumptions and boundary conditions

The assumptions and boundary conditions adopted in this study are described in this section.

2.6.1. Data center, cooling system, and photovoltaic power plant

The DC electric demand is assumed as constant and equal to 200 kW (Fig. 5), in line with data provided by Ajayi and Heyman [2], and 97 % of the DC electric consumption is converted into waste heat [29] available at 50 °C. The released waste heat needs to be removed through a cooling system. This one is assumed relying on passive free cooling technologies, i.e., direct airside economization and direct waterside economization (through the use of a chiller), depending on the instantaneous ambient temperature and consistently with the more efficient passive cooling technologies outlined in the cooling strategies for DC review by Nadjahi et al. [30]. The fans are allowed to work only when ambient air temperature is below 15 °C [29], and are assumed to work at an equivalent constant COP equal to 20 [30]. The equivalent COP for the fans is defined as the ratio between the thermal energy removed and the electric consumption, as the chiller COP, which is assumed constant and equal to 4, in line with the data provided by Sathesh and Shih [31].

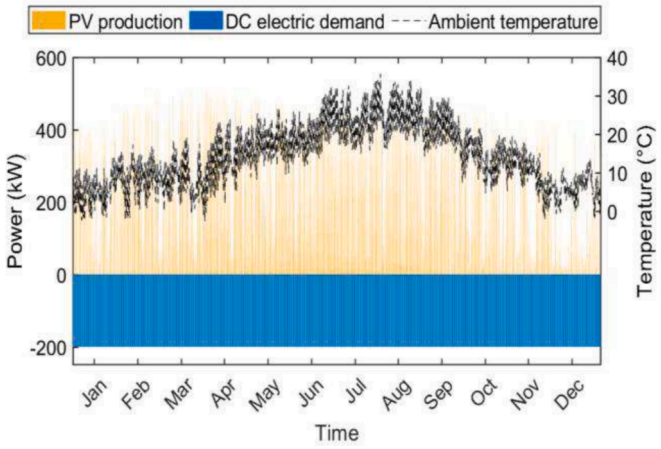

Fig. 5. Boundary conditions: power (PV production and DC electric demand) and ambient temperature profiles.

Photovoltaic solar panels with a total surface of 2000 m^2 are considered in this study as the renewable power source. The PV plant is sized to widely fulfil the DC energy demand. In a previous study of the Authors [26] investigating the integration between CB and PV, a sensitivity analysis was performed on the PV size, highlighting that the size parameter is not significantly affecting the CB performance. The PV production (Fig. 5), at each time step (15 min), has been calculated adopting the irradiance hourly profile, G, in Bologna (Italy) during the year 2020, as the assumed ambient temperature hourly profile [32]. The ambient temperature, T_{amb}, (Fig. 5) influences the panels temperature, T_{PV}, according to Eq. (27) [33], the ORC performance and the thermal losses to the environment occurring in the TES.

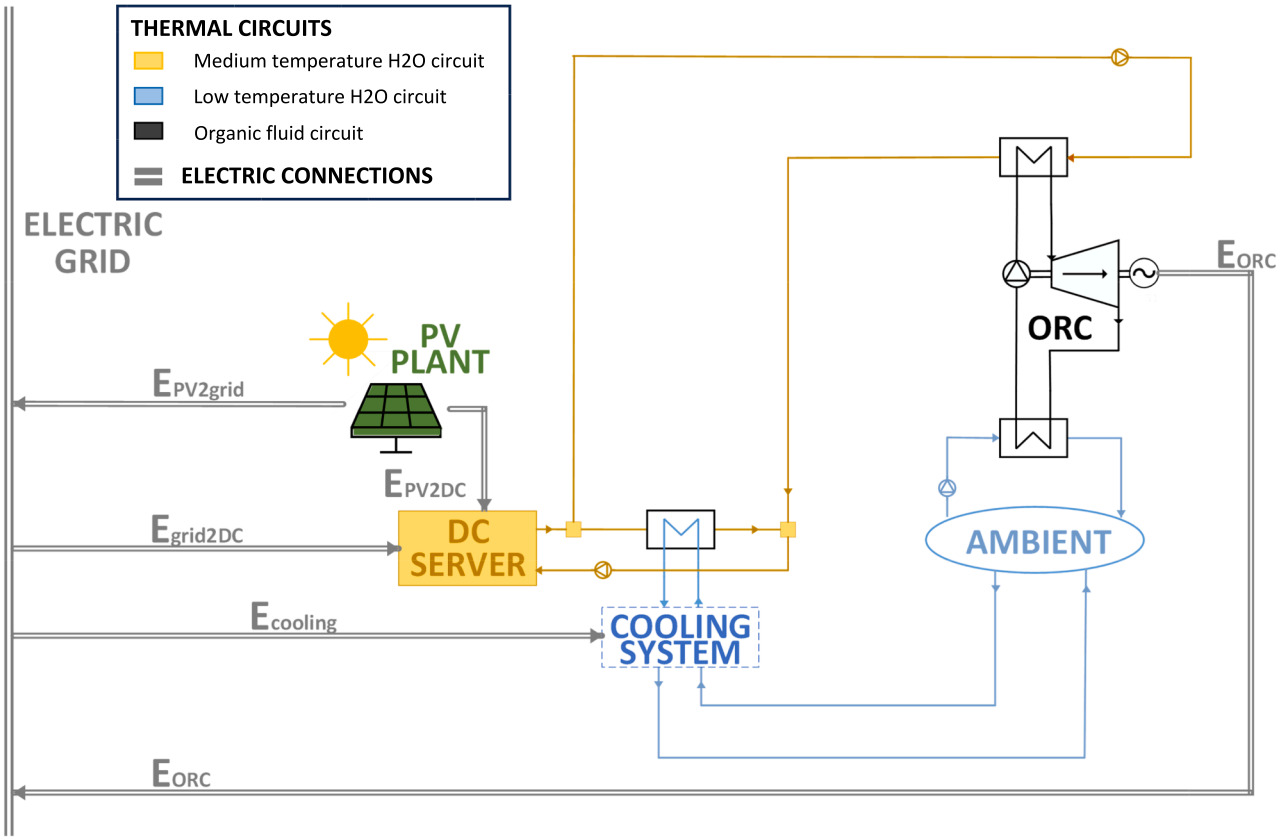

Fig. 4. ORC-only system configuration layout, where the main components, the thermal circuit, and the electric connections are shown.

$$T_{PV} = T_{amb} + \frac{G}{G_{ref}}\left(T_{NOCT} - T_{ref}\right) \quad (27)$$

In Eq. (27), the reference irradiance G_{ref} and temperature T_{ref} values are respectively considered equal to 800 W/m^2 and 20 °C, according to [33]. T_{NOCT} is the nominal operating cell temperature, assumed equal to 45 °C [34].

The panels temperature, T_{PV}, affects also the PV efficiency, η_{PV}, according to the following general equation [33]:

$$\eta_{PV} = \eta_{ref}\left[1 - \beta_{ref}\left(T_{PV} - T_{ref}\right) + \gamma log(G)\right] \quad (28)$$

where η_{ref} is the PV nominal efficiency assumed equal to 25 % [34], β_{ref} is the temperature coefficient equal to 0.26 %/°C [34], and γ is the irradiance coefficient, considered null according to [35].

The thermal user in the reference system is assumed to require thermal energy at 80 °C. All the hypotheses and boundary conditions of this study are summarized in Table 3.

2.6.2. Thermodynamic analysis boundary conditions

The thermodynamic analysis is performed by comparing a set of fluids, which presents thermodynamic and environmental properties suitable for the investigated application. Since the DC waste heat is available at 50 °C, considering a plausible temperature lift for the HP [36] and the characteristics of the reference CB [21], the fluids are selected with a critical temperature in the range between 90 and 200 °C. Furthermore, all the fluids with high critical pressure (> 50 bar) are discarded. Eventually, only environmentally friendly fluids (with low Global Warming Potential – GWP – and null Ozone Depletion Potential – ODP) are considered in the selected set. R134a and R245fa are also included in the set of fluids, as conventional HFC reference fluids for the considered range of operating temperature for ORC [37]. Table 4 shows the selected set of fluids, and the corresponding critical temperature, critical pressure, ODP and GWP100 values.

The input quantities set in the thermodynamic constant-efficiency model are listed in Table 5. The selected values are chosen in line with the application of the CB to the DC cooling system, according to the operating conditions of the reference prototype [21], and adopted in similar thermodynamic models [36]. More in detail, cold source/sink temperature values correspond to DC waste heat temperature (50 °C) in HP mode, and to an average ambient temperature (25 °C) in ORC mode. The hot sink/source temperature values are chosen according to the temperature available in the TES in the prototype [22] and considered as a reference in the semi-empirical model. The isentropic efficiency values of the HP and ORC machines and the secondary fluids' glide values also match the reference prototype values. Minimum pinch point, superheating and subcooling degrees are chosen in line with similar thermodynamic models [36].

2.6.3. Carnot battery parameters

The HP/ORC parameters and constraints, listed in Table 6, derive from the characteristics of a reference CB test bench [21]. The adopted

Table 3
DC, cooling system, and PV hypotheses.

Data Center	
IT + lighting and auxiliaries electric consumption (kW)	200
Electricity converted into WH (%)	97
WH Temp. (°C) $-T_{WH}$	50
Cooling System	
COP chiller (−)	4
COP fans (−)	20
Max Temp. to use fans (°C)	15
PV Solar Panels	
Area (m^2)	2000
Nominal efficiency (%)	25
TH user min Temp. (°C) $-T_{TH,min}$	80

Table 4
Working fluid selected set [18].

Fluid Name	T_{crit} (°C)	p_{crit} (bar)	ODP (−)	GWP100 (−)
HFE143m	104.77	36.350	0	0
Isobutane	134.67	36.290	–	–
Isobutene	144.94	40.098	–	–
Isopentane	187.20	33.780	–	–
n-Butane	151.98	37.960	–	3
n-Pentane	196.55	33.700	–	–
n-Propane	96.74	42.512	–	3
Neopentane	160.59	31.960	–	–
Novec649	168.66	18.690	–	–
R1233zd(E)	166.45	36.236	0	0
R1234yf	94.70	33.822	–	4
R1234ze(E)	109.37	36.363	–	6
R1234ze(Z)	150.12	35.330	0	0
R13I1	123.29	39.526	–	0.4
R134a	101.06	40.593	–	1430
R152A	113.26	45.200	–	124
R245ca	174.42	39.407	–	–
R245fa	153.86	36.510	–	1030

electric power size equal to 25 kW is a compromise between the HP size that allows absorbing the entire thermal power released by the DC in HP mode (calculated according to the methodology explained in subsection 2.2) and the associated storage feasible sizes. Indeed, considering R1233zd(E) as the working fluid according to the reference test bench, the electric size of the HP that would exploit the entire thermal power released by the DC would be equal to 50 kW (Fig. 6). The CB size in the model is rescaled considering the same efficiencies for the same boundary conditions.

A cylindrical tank with an aspect ratio (height to diameter ratio) of 6 has been considered as TES, to improve the charging and discharging efficiency, according to [38]. The storage volume has been varied from 5 to 30 m^3 with a step of 5 m^3 and discretized in 20 layers (Table 6).

The values of the cost parameters are listed in Table 7, including the CB investment cost with the associated lifetime, the discounted rate adopted for the actualization of the investment, and the thermal energy price, considered constant during the year. More in detail, for the reversible HP/ORC system a specific investment cost of 2500 €/kWe has been considered according to Lemmens [39] for a size of 25 kW. In general, the investment cost of a HP/ORC system could be affected by several design choices, including the machine's invertibility, the components' size, the thermodynamic settings and the adopted working fluid. In this reference study, the electric power size has been considered the main clear and simple driver of the specific investment cost, adopting the correlation reported in [39]. The storage investment cost varies with the volume, and it has been calculated according to Shamoushaki et al. [40]. The lifetime and the discounted rate values derive from [41]. The thermal energy price is assumed constant and equal to 0.08 and 0.16 €/kWh respectively in the years 2018 and 2022, according to the average district heating thermal energy price that occurred in Bologna (Italy) in the reference years [42]. The electricity price profile derives from the hourly spot market values that occurred in the North of Italy in 2018 and 2022 [43]. Two scenarios with very different energy prices (Fig. 7) have been analysed. In the following sections, the two scenarios will be referred to as respectively the "low energy price" scenario and the "high energy price" scenario.

In the ORC-only case, all the hypotheses and the parameters' values are unchanged, except for the constraint on the ORC minimum operating temperature ($T_{ORC,min}$), which is removed, since the heat source is constantly available at 50 °C. The technical feasibility of ORCs working with such low heat source temperature benches has already been experimentally assessed for a 3 kWe-size [44] and an 11 kWe-size [45] ORC test bench.

Table 5
Inputs set in the thermodynamic model.

$\eta_{is,comp}$(−)	$\eta_{is,exp}$(−)	$\eta_{is,pump}$(−)	ΔT_{pp}(K)	SH(K)	SC(K)	TH_{in}(°C)	TC_{in}(°C)	sfH_{glide}(K)	sfC_{glide}(K)
0.70	0.75	0.65	3	5	5	85/90 (HP/ORC)	50/25 (HP/ORC)	5	5

Table 6
Carnot battery parameters.

Reversible HP/ORC	
Nominal electric Power (kW)	25
Max op. Temp. (°C) $-T_{TES,max}$	95
ORC min op. Temp. (°C) $-T_{ORC,min}$	60
HP cold sink Temp. (°C)	50
TES	
Volume (m^3)	from 5 to 30
Aspect ratio (−)	6
N° of Mixing Zones (−)	20
Wall Th. Resistance (m^2· K/W)	10
Initial Temp. (°C)	95
Op Temp. range (°C)	60–95

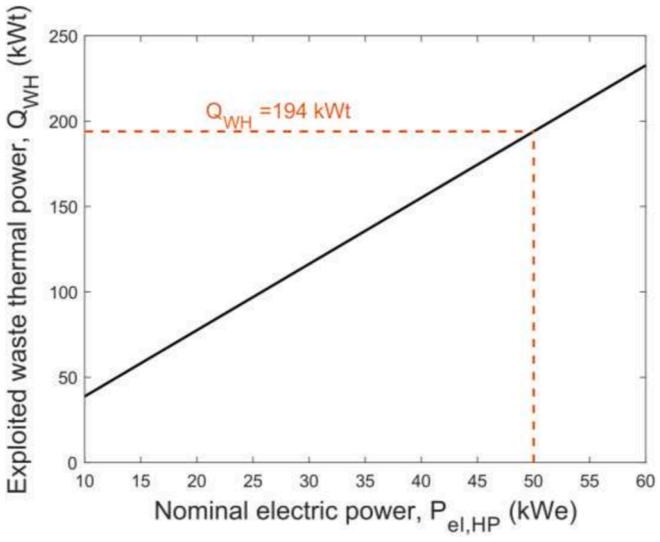

Fig. 6. Absorbed thermal power versus HP electric consumption in nominal conditions.

Table 7
Cost parameters.

Cost parameters	
HP/ORC cost (€/kWe)	2500
Storage cost (€) [40]	
Lifetime (years)	20
Discounted rate (%) − r	6
Thermal energy price (€/kWh)	0.08 / 0.16

2.7. Performance indexes

The performance indexes adopted to compare the fluids performance are the thermodynamic coefficient of performance (COP_{th}), defined according to Eq. (11), the net thermodynamic efficiency ($\eta_{ORC,th}$), defined according to Eq. (22), and the thermodynamic roundtrip efficiency ($\eta_{rt,th}$), defined as it follows:

$$\eta_{rt,th} = COP_{th} \bullet \eta_{ORC,th} \tag{29}$$

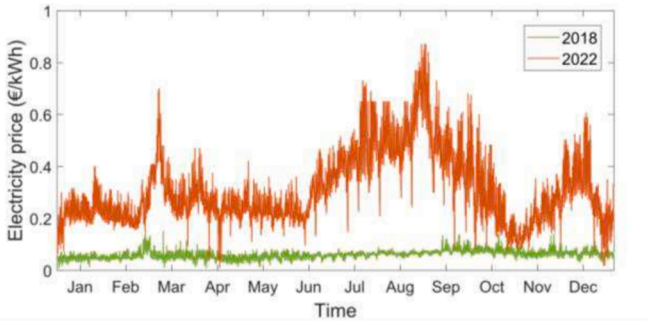

Fig. 7. Yearly electricity cost profiles.

For the sake of simplicity, since Eq. (29) is adopted for working fluid comparison only, the storage tank is considered completely insulated (adiabatic), thus with unitary storage efficiency.

The CB operation, when integrated in the reference application, is evaluated through:

i) the annual electric energy consumed by the HP (E_{HP}) and produced by the ORC (E_{ORC});

ii) the annual thermal energy produced by the HP (Q_{HP}) and absorbed by the ORC (Q_{ORC});

iii) the CB annual running hours in HP and ORC modes;

iv) the annual average COP/efficiency (η_{ORC}), defined respectively for the HP mode and for the ORC mode, according to Eq. (30) and (31).

$$COP = \frac{\sum Q_{HP}}{\sum E_{HP}} \tag{30}$$

$$\eta_{ORC} = \frac{\sum E_{ORC}}{\sum Q_{ORC}} \tag{31}$$

v) The overall performance is provided by the yearly average roundtrip efficiency, η_{rt} (Eq. (32)), in which the storage efficiency is defined according to Eq. (33).

$$\eta_{rt} = COP \bullet \eta_{ORC} \bullet \eta_{TES} \tag{32}$$

$$\eta_{TES} = \frac{\sum Q_{ORC} + \sum Q_{TH}}{\sum Q_{HP}} \tag{33}$$

The techno-economic performance of the integrated system is analysed through the additional revenues and expenses due to the CB integration into the system. The yearly economic gain (C_{year}) is obtained by summing the gain, ΔC (Eq. (26)), at each timestep.

$$C_{year} = \sum\nolimits_{year} \Delta C \tag{34}$$

The payback period, in the forms of simple payback period (SPB) and discounted payback period (DPB), is evaluated according to Eq. (35) and (36).

$$SPB = \frac{I_{HP/ORC} + I_{TES}}{\sum \Delta C} \tag{35}$$

$$\sum_{t=1}^{DPB} \frac{\sum \Delta C}{(1+r)^t} = I_{HP/ORC} + I_{TES} \tag{36}$$

where $I_{HP/ORC}$ and I_{TES} are the investment cost of the HP/ORC and

storage, r is the discount rate and ΔC is the yearly economic differential gain.

The DC and cooling system performance improvement is assessed by evaluating the Power Usage Effectiveness (PUE) and the Energy Reuse Effectiveness (ERE) described respectively in Eq. (37) and (38), according to [30].

$$PUE = \frac{E_{cooling} + E_{light\&loss} + E_{IT}}{E_{IT}} \tag{37}$$

$$ERE = \frac{E_{cooling} + E_{light\&loss} + E_{IT} - E_{reuse}}{E_{IT}} \tag{38}$$

where $E_{cooling}$ is the electricity required to cool down the servers, $E_{light\&loss}$ is the electricity lost in the energy distribution system and in other infrastructures (UPS or PDU) and to light the DC, E_{IT} is the input energy of the IT equipment, and E_{reuse} is the recovered thermal energy.

Eventually, the cooling system reduction of load, due to a partial use of the HP to cool down the DC, is described by the utilization factor (UF), which is the ratio between the cooling energy associated with the chiller and the fans in the two scenarios with ($E_{cooling,chiller/fans}$) and without ($E_{cooling,chiller/fans,noCB}$) the CB intervention.

$$UF_{chiller/fans} = \frac{E_{cooling,chiller/fans}}{E_{cooling,chiller/fans,noCB}} \tag{39}$$

The ORC-only configuration technical feasibility is evaluated by comparing the ORC performance in terms of annual electricity production, thermal consumption, average efficiency and running hours, with the ORC performance when integrated into the CB. Furthermore, the yearly economic gain in case of ORC-only configuration, $C_{year,ORC}$ (Eq. (40)), the PUE (Eq. (37)), the ERE (Eq. (38)) and the UF (Eq. (39)) are assessed.

$$C_{year,ORC} = \sum_{year} E_{ORC} \bullet C_{el} \tag{40}$$

3. Results and discussion

This section presents and discusses the results of the analysis. The thermodynamic performance results of the selected fluids are shown in terms of thermodynamic COP, ORC efficiency, and roundtrip efficiency. The techno-economic performance of a CB integrated with the cooling system of a DC feed by a PV power plant is shown for different sizes of the storage volume, and for two different scenarios of the energy price. Furthermore, the improvement of the integrated system's overall performance due to the operation of the CB is assessed. The economic benefit provided by the CB integration is compared to the gain obtainable with the ORC-only configuration.

3.1. Thermodynamic design analysis results

The selected suitable fluids for the DC application (Table 4) are compared in terms of thermodynamic performance through the thermodynamic model described in section 2.2. The thermodynamic COP, ORC efficiency, and roundtrip efficiency, obtained with the selected fluids, inputs and parameters in Table 5, are provided in Fig. 8.

The COP_{th} values are in the range 3.2–4.8, and the $\eta_{ORC,th}$ values are in the range between 7.4 % and 8.9 %. As a result, the $\eta_{rt,th}$ values range between 25 % and 43 %. Results indicate that the olefin R1233zd(E) outperforms all the other fluids both in HP and ORC modes, showing the highest COP_{th} and $\eta_{ORC,th}$, equal respectively to 4.78 and 8.91 %. For this reason, it is not convenient to use different working fluids for the two different modes (HP mode and ORC mode). The corresponding $\eta_{rt,th}$ value reaches 42.6 %. This value is lower than roundtrip efficiency values reached by storage technologies such as pumped hydro energy storage, chemical batteries, flywheel energy storage, compressed air energy storage and others [46], but it is comparable with hydrogen energy storage roundtrip efficiencies available in literature [47]. The pressure and temperature values obtained for the HP cycle and ORC using R1233zd(E) are listed in Table 8.

3.2. Techno-economic assessment of the Carnot battery intervention in the reference system

In this subsection, the benefit obtainable with the integration of the reference CB in the DC cooling system is discussed in terms of techno-economic performance of the CB, and overall system performance.

3.2.1. Integrated system weekly operation

Fig. 9 and Fig. 10 show the integrated system energy flows in terms of electric (a) and thermal (b) power for two representative weeks, one in winter (Fig. 9), and one in summer, (Fig. 10). The system electric and thermal production values are considered positive, while the system demand/consumption values are shown as negative.

Fig. 9(a) and Fig. 10(a) show the electric energy flows in the integrated system. The PV production (in yellow) depends on the solar radiation; the DC electric demand (in blue) is constant; the chiller (in light

Table 8
Pressure and temperature values of the HP cycle and ORC obtained with R1233zd(E).

	p_v(bar)	p_k(bar)	T_1(°C)	T_2(°C)	T_3(°C)	T_4(°C)
HP	2.3	8.5	47	94	86	42
ORC	7.2	1.7	90	53	28	26

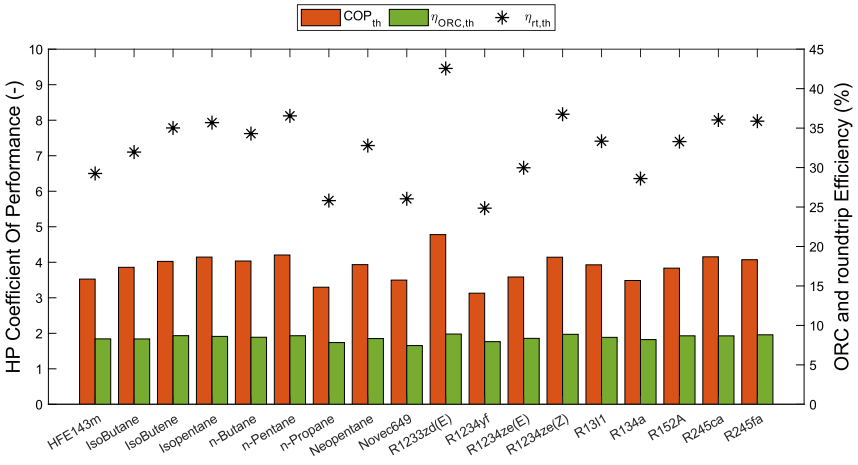

Fig. 8. Thermodynamic performance comparison of the selected fluids.

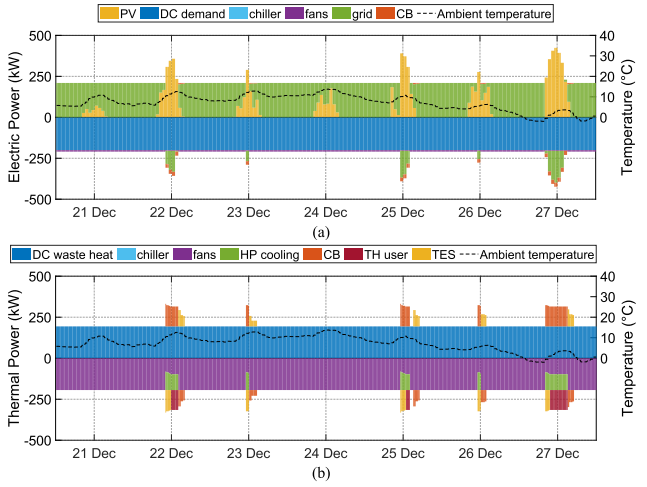

Fig. 9. Electric (a) and thermal (b) energy flows in a typical winter week.

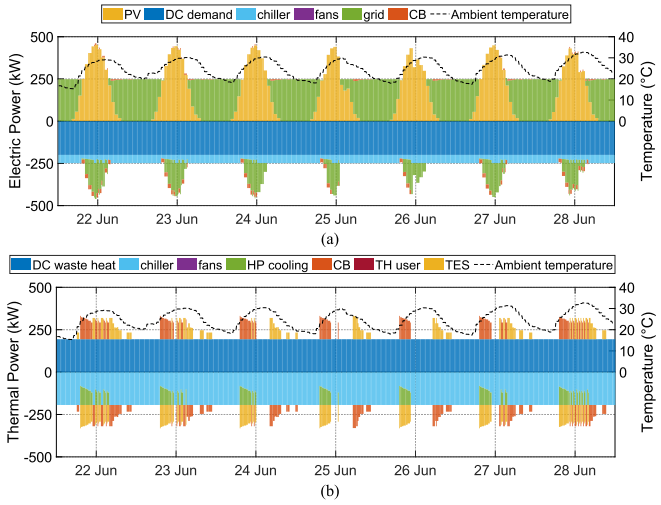

Fig. 10. Electric (a) and thermal (b) energy flows in a typical summer week.

blue) and fans (in purple) electric consumptions are included respectively in summertime and wintertime; the CB electric power (in orange) assumes negative values when it represents the HP electric consumption, and positive values when it represents the ORC electric production; the electric power from/to the grid (in green) assumes positive values when it enters the system to cover the consumption/demand, and negative values when it is produced and sold to the grid. Fig. 9(b) and Fig. 10(b) show the thermal energy flows in the integrated system. The DC waste heat (in blue) production is constant; the chiller (in light blue), fans (in purple) and HP (in green) cooling power is assumed as negative because it represents thermal power removed from the system; the CB thermal power (in orange) is positive when it is the HP thermal production, and negative when it is absorbed by the ORC; the thermal power delivered to the thermal user is shown in red; the thermal power entering and exiting the storage (TES) is represented in yellow and with the opposite sign compared to the CB thermal power.

In wintertime, as the PV production is low, most of the DC demand needs to be covered by the grid (Fig. 9(a)). When there is a surplus in the PV production, the HP is run (in orange), first to fill the storage (in yellow with the negative sign, in Fig. 9(b)) and then to produce thermal energy to sell to the thermal user (in red). This strategy is applied to minimize the cooling system load, through the maximization of the HP utilization, and to maximize the DC waste heat recovery. Then, when the PV production decreases, the ORC (in orange) is run until the storage is empty (positive yellow bars in Fig. 9(b) representing thermal energy stored in the TES).

In summertime, assuming no thermal demand, the HP (in orange) is not allowed to run as long as there is an electric surplus (see Fig. 10(a)) because the storage gets full (in yellow in Fig. 10(b)). Thus, the ORC is run alternatively to the HP to produce an electric surplus to sell to the grid, discharging the storage and allowing the HP to run later. When the HP works, there is a reduction of the load on the cooling system (in green in both Fig. 9(b) and Fig. 10(b)).

Furthermore, in wintertime, when the ambient temperature is low (typically below 15 °C), only the fans are activated as the cooling system (Fig. 9), while in summertime the chiller is necessary, leading to higher electric consumption (Fig. 10).

3.2.2. *Carnot battery techno-economic performance*

The additional annual revenues and expenses, resulting from the integration of the CB into the reference system, are presented in Fig. 11 and Fig. 12, for the two energy price scenarios. An enlargement of the storage volume results in an intensification of the energy storage capacity, which allows an extension of the CB operational time, enhancing the decoupling of the DC electric demand and the PV power production. Therefore, since the increase in the storage capacity makes a larger amount of thermal energy available, a notable boost in the ORC production occurs. The HP electric consumption experiences a marginal increase until reaching a specific size of the storage volume (25 m^3), after which it stabilizes. This stabilization occurs because the HP reaches its maximum production capacity based on surplus renewable electricity. To clarify, with a storage volume smaller than 25 m^3, the HP operation may be hindered if the storage is full, in case of renewable surplus. With a larger storage volume (30 m^3), the HP operation is no longer constrained by the storage size, but rather depends on the availability of surplus renewable energy, in addition to temperature constraints. The increase in ORC production comes at the expense of reduced thermal production, as the storage volume is scaled up. The savings from the cooling system, realized when using the HP to absorb DC waste heat, rise with the HP production and the storage volume. Notably, in the high energy price scenario, the enhancement in savings becomes more pronounced due to a substantial augmentation in the electricity price.

The yearly economic gain (due to the operating revenues and expenses), SPB and DPB values, obtainable in the two energy price scenarios, are listed respectively in Table 9 and Table 10. SPB and DPB values higher than the CB lifetime (20 years) are not specified in the tables. In the case of low energy prices, the integration of a CB to the system is deemed economically unfavourable, requiring an extended

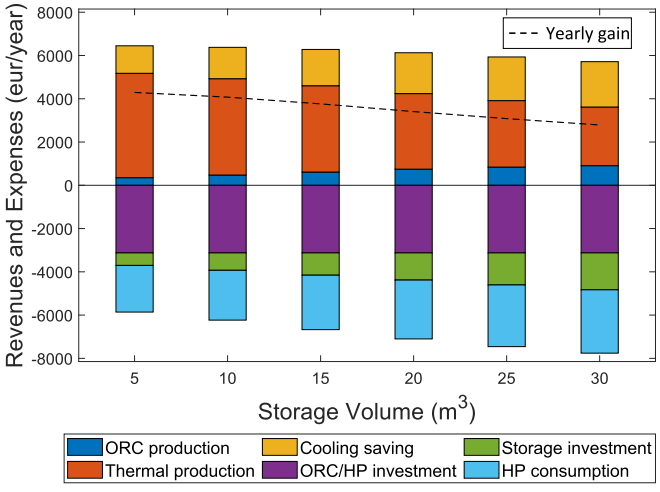

Fig. 11. Economic gain due to the CB (low energy price scenario).

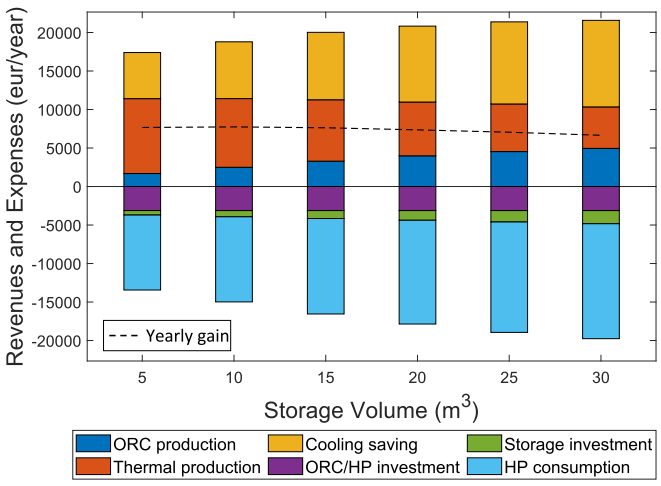

Fig. 12. Economic gain due to the CB (high energy price scenario).

Table 9
Yearly economic gain, simple and discounted payback period (low energy price scenario).

Storage volume (m^3)	5	10	15	20	25	30
Yearly gain (€/year)	4292	4075	3763	3407	3082	2788
SPB (years)	17.3	19.3	> 20	> 20	> 20	> 20
DPB (years)	> 20	> 20	> 20	> 20	> 20	> 20

Table 10
Yearly economic gain, simple and discounted payback period (high energy price scenario).

Storage volume (m^3)	5	10	15	20	25	30
Yearly gain (€/year)	7668	7744	7631	7356	7051	6655
SPB (years)	9.66	10.1	10.9	11.9	13.1	14.5
DPB (years)	13.6	14.7	16.5	19.2	> 20	> 20

period to recover the investment cost (Table 9). Conversely, with an increase in energy prices, the integrated system featuring the CB becomes an attractive solution, at least for smaller storage capacities. The payback period sees a significant reduction, reaching compelling values, especially for relatively compact storage volumes (Table 10).

Table 11 offers a comparison of the performance of the CB in the two energy price scenarios, considering a storage volume of 10 m^3, which represents the value that maximizes the yearly economic gain (C_{year}) occurred in the high energy price scenario (7744 €/year).

More encouraging values of the yearly economic gain, SPB and DPB are obtained in the two energy price scenarios when the possibility of selling the electricity to the grid is not available (Table 12 and Table 13). In this way, the HP consumption is not considered anymore as an expense because the associated energy would be dissipated in the absence of the CB, and the ORC production would be possible only for self-consumption. These results are particularly interesting, especially in

Table 12
Yearly economic gain, simple and discounted payback period when selling the electricity to the grid is not possible (low energy price scenario).

Storage volume (m3)	5	10	15	20	25	30
Yearly gain (€/year)	6337	6306	6232	6091	5909	5703
SPB (years)	11.7	12.4	13.3	14.4	15.6	16.9
DPB (years)	18.6	> 20	> 20	> 20	> 20	> 20

Table 13
Yearly economic gain, and discounted payback period when selling the electricity to the grid is not possible (high energy price scenario).

Storage volume (m3)	5	10	15	20	25	30
Yearly gain (€/year)	16,988	18,491	19,820	20,691	21,283	21,524
SPB (years)	4.36	4.25	4.19	4.23	4.33	4.49
DPB (years)	4.87	4.73	4.66	4.71	4.83	5.03

the high energy price scenario (Table 13), in which the payback reaches values between 4 and 5 years, making the proposed CB integration economically feasible.

3.2.3. Integrated system overall performance

The intervention of the CB results in enhancements in both the DC PUE and ERE, as illustrated in Fig. 13. This improvement stems from the HP contributing to a portion of the cooling power, and approximately 30 % of the HP electric consumption (not used as thermal energy) is recovered by the ORC, as indicated in Table 11 (η_{lrt} is close to 30 %). With the CB operation, the running hours increase with the storage volume, leading to a corresponding improvement in both PUE and ERE. Furthermore, the augmentation of storage capacity facilitates a

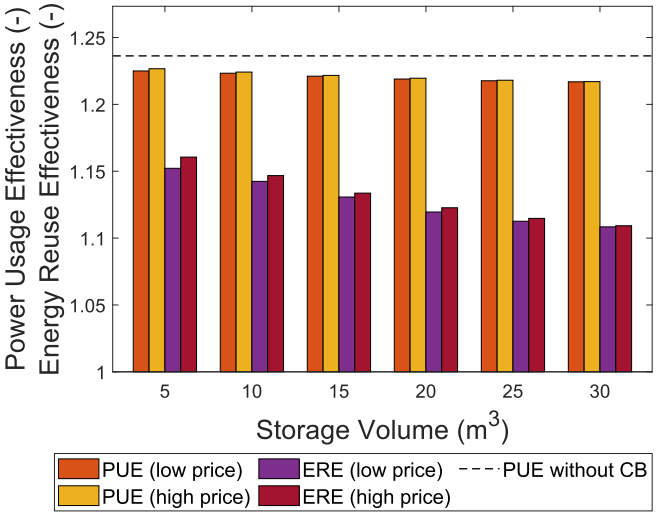

Fig. 13. PUE and ERE.

Table 11
CB performance for a storage volume of 10 m^3.

	Low energy price scenario			High energy price scenario			PV
	HP	ORC	TH dis.	HP	ORC	TH dis.	
Annual average COP/efficiency (–)/(%)	4.88	7.05	–	4.90	7.16	–	20.5
Annual electrical energy (kWh)	36,543	7140	–	34,778	6774	–	870,769
Annual thermal energy (kWh)	178,247	101,292	55,667	170,410	94,656	55,761	–
Annual running hours (h)	1497	1230	459	1425	1169	460	4267
Annual average storage efficiency (%)	88.1	–	88.3	–	–		
Annual average roundtrip efficiency (%)	30.3	–	31.0	–	–		

reduction in the required cooling system power, especially of the chiller, which is more energy-intensive due to the lower *COP*, as highlighted in Fig. 14 through the *UF*. In conclusion, the overall performance of the integrated system improves with the CB use, regardless of the energy price.

3.3. ORC-only configuration performance assessment

In the ORC-only configuration, the ORC is forced to work always in strongly off-design conditions, due to the very low heat source temperature. Furthermore, the high ambient temperatures occurring in summertime prevent the ORC from being activated for most of the time occurring between June and September. The ORC performance in the ORC-only configuration is shown in Table 14, including the ORC performance when integrated into the CB for the sake of comparison.

Results show that the ORC annual average efficiency significantly drops down in the ORC-only configuration, due to the strongly off-design conditions in which the ORC operates. Although the working hours in the ORC-only configuration are more than three times the working hours in the CB configuration, the significantly lower temperature of the heat source allows the recovery of less thermal power, which results in only slightly higher annual thermal energy. Furthermore, the lower efficiency allows the production of a lower amount of electricity compared to the CB configuration.

Fig. 15 shows the revenues and the expenses associated with the ORC-only configuration. The revenues are due to the ORC electric production that contributes to cover the DC energy requirements, and the reduction of the cooling system load through the ORC evaporator absorbing part of the waste heat. The expenses are related to the ORC investment cost (levelized value in Fig. 15). In both the energy price scenarios (even if in different proportions), the yearly expenses are higher than the revenues. Thus, the SPB and DPB are higher than the ORC lifespan. The annual gain of the ORC, associated with the operating costs, is detailed in Table 15 for the two energy price scenarios. The DC PUE and ERE, and the cooling system UF, listed in Table 15, are the same in the two scenarios because they are not affected by the energy price.

4. Conclusions

This study contributes to the existing body of literature on the implementation of CBs in technologies for recovering waste heat from data centers. It involves simulating the integration of a reversible HP/ORC Carnot battery in the cooling system of DC, powered by the electricity generated from a PV power plant.

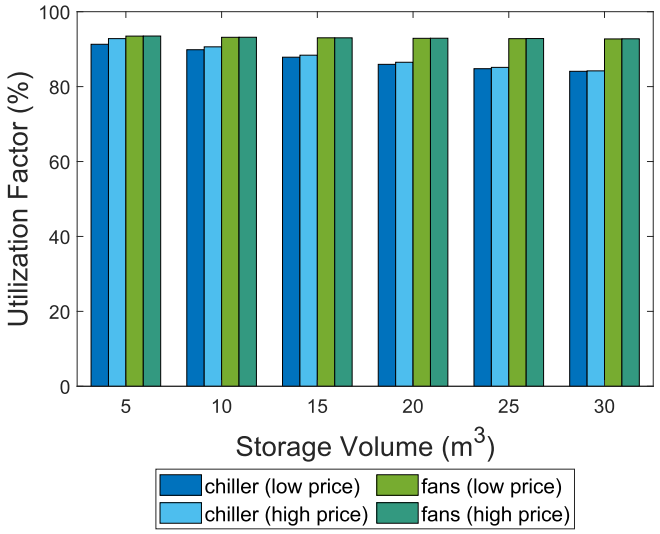

Fig. 14. Utilization factor.

Table 14
ORC performance in CB and in ORC-only configurations.

	Low energy price scenario		High energy price scenario	
	ORC in CB	ORC-only	ORC in CB	ORC-only
Annual average efficiency (%)	7.05	1.53	7.16	1.53
Annual electrical energy (kWh)	7140	4366	6774	4366
Annual thermal energy (kWh)	101,292	126,512	94,656	126,512
Annual running hours (h)	1230	3971	1169	3971

The initial part of this investigation involves conducting a thermodynamic performance analysis to identify the optimal working fluid for the intended application. The highest performing fluid results to be R1233zd(E) in both the HP cycle and ORC, enabling the achievement of a thermodynamic roundtrip efficiency of 43 %, assuming the operating conditions typical for the considered application.

Subsequently, in the second part of the study, a comprehensive semi-empirical off-design model of a CB is utilized within a rule-based control strategy to manage the operations of the ORC and HP in the integrated system. In instances where the PV panels generate excess electricity, this surplus energy can be stored in the CB through the HP, concurrently reducing the load and consumption of the cooling system. When the demand exceeds the renewable production, the stored thermal energy is employed to operate the ORC. Additionally, in winter, the option to sell the stored thermal energy to an external thermal user is included. A sensitivity analysis varying both the storage volume and the energy price is conducted to identify the optimal compromise for the storage size and explore the impact of the storage capacity and energy price on the integrated system. Results indicate that integrating the CB can be economically viable in the high energy price scenario, even though the impossibility for the CB to absorb electricity from the grid when operating in HP mode (conservative hypothesis). With a storage capacity of 10 m^3, the annual additional profit is estimated to be approximately 7744 €, and the simple payback period is about 10 years. More interesting results are obtained when selling the produced electricity to the grid is not possible. Indeed, a payback period of less than 5 years is reached with a yearly economic gain of almost 18,500 € (considering the same storage size) in the high energy price scenario. Furthermore, the conservative assumptions governing the CB operation, along with the validation of the model on a non-optimized prototype plant, leave a margin for enhancing the overall performance and the economic benefit. The thermal integration enables the achievement of roundtrip efficiencies of more than 30 %, although the very low operating temperatures. As the HP contributes to satisfying the cooling load, and a portion of the HP electric consumption is recovered by the ORC, the data center PUE and ERE see improvements with the CB integration.

In the last part of the work, the CB integration is compared with the less complex alternative in which the DC waste heat is continuously recovered through an ORC system. In this configuration, the integrated ORC is identical in size and characteristics to the ORC involved in the CB configuration. The results available from the comparison show a significant drop in the ORC technical performance and the system's overall economic feasibility. Indeed, the ORC annual average efficiency drops to 1.5 % due to i) the very low heat source temperature, which significantly decreases the thermodynamic efficiency, and ii) the strongly off-design conditions in which the ORC is forced to operate. Furthermore, even if the ORC is set to operate continuously during the year, for more than half of the year, the ambient temperature is too high to ensure a temperature difference between the hot source and the cold sink high enough to run the ORC. The results from this last comparison encourage the utilization of a more complex system as a CB, instead of an ORC, for DC waste heat recovery application. In this regard, it is important to

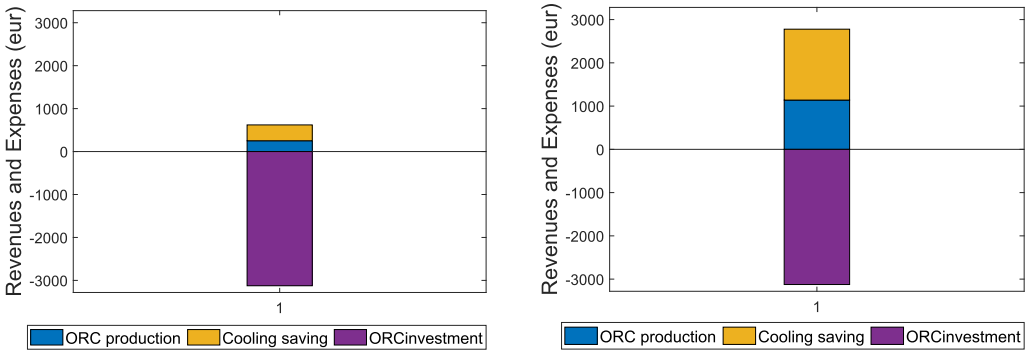

Fig. 15. Economic gain in ORC-only configuration in (a) high energy price and (b) low energy price scenarios.

Table 15
ORC-only configuration overall performance.

	Low energy price scenario	High energy price scenario	Case without ORC
Yearly economic gain (€/year)	620	2778	–
SPB (years)	> 20	> 20	–
DPB (years)	> 20	> 20	–
PUE (–)	1.233		1.236
ERE (–)	1.160		–
UF chiller (–)	1		1
UF fans (–)	0.86		1

highlight that a CB is an electric energy storage, so it can be considerable only in presence of renewable electricity production.

4.1. Future developments

In terms of future advancements, the potential of buying electricity from the grid during periods of low prices to power the HP will be explored. This strategic consideration aims to further optimize the system's energy efficiency and financial performance. Additionally, the dynamic inertia of the system when transitioning between different operating modes of the CB can be included in the system modelling. This adjustment is crucial for ensuring a smoother and more responsive adaptation to varying conditions, enhancing the overall reliability and performance of the integrated system.

Declaration of competing interest

The authors declare that they have no known competing financial interests or personal relationships that could have appeared to influence the work reported in this paper.

Acknowledgements

The Authors thank the 7th International Seminar on ORC Power Systems ORC2023 conference, September 2023, Seville.

Data availability

Data will be made available on request.

References

[1] Q. Huang, S. Shao, H. Zhang, C. Tian, Development and composition of a data center heat recovery system and evaluation of annual operation performance, Energy 189©, Art. no. C, 2019, Accessed: Mar. 16, 2022. [Online]. Available: https://ideas.repec.org/a/eee/energy/v189y2019ics036054421931895x.html.

[2] O. Ajayi, R. Heymann, Data centre day-ahead energy demand prediction and energy dispatch with solar PV integration, Energy Rep. 7 (2021) 3760–3774, https://doi.org/10.1016/j.egyr.2021.06.062.

[3] J. Cho, T. Lim, B.S. Kim, Viability of datacenter cooling systems for energy efficiency in temperate or subtropical regions: case study, Energ. Build. 55 (Dec. 2012) 189–197, https://doi.org/10.1016/j.enbuild.2012.08.012.

[4] G.D. Chethana, B. Sadashive Gowda, Thermal management of air and liquid cooled data centres: a review, Mater. Today: Proc. 45 (2021) 145–149, doi: 10.1016/j.matpr.2020.10.396.

[5] Z.M. Marshall, J. Duquette, A techno-economic evaluation of low global warming potential heat pump assisted organic Rankine cycle systems for data center waste heat recovery, *Energy* 242 (Mar. 2022) 122528, https://doi.org/10.1016/j.energy.2021.122528.

[6] K. Ebrahimi, G.F. Jones, A.S. Fleischer, A review of data center cooling technology, operating conditions and the corresponding low-grade waste heat recovery opportunities, *Renew. Sustain. Energy Rev.* 31 (Mar. 2014) 622–638, https://doi.org/10.1016/j.rser.2013.12.007.

[7] K. Ebrahimi, G.F. Jones, A.S. Fleischer, The viability of ultra low temperature waste heat recovery using organic Rankine cycle in dual loop data center applications, *Appl. Therm. Eng.* 126 (Nov. 2017) 393–406, https://doi.org/10.1016/j.applthermaleng.2017.07.001.

[8] M. R. Jawad Al-Tameemi, Y. Liang, Z. Yu, Combined ORC-HP thermodynamic cycles for DC cooling and waste heat recovery for central heating, Energy Procedia, vol. 158, pp. 2046–2051, Feb. 2019, doi: 10.1016/j.egypro.2019.01.471.

[9] M. Temiz, I. Dincer, A newly developed solar-based cogeneration system with energy storage and heat recovery for sustainable data centers: energy and exergy analyses, Sustain. Energy Technol. Assess. 52 (Aug. 2022) 102145, https://doi.org/10.1016/j.seta.2022.102145.

[10] Y. Jang, D. Lee, J. Kim, S.H. Ham, Y. Kim, Performance characteristics of a waste-heat recovery water-source heat pump system designed for data centers and residential area in the heating dominated region, J. Build. Eng. 62 (Dec. 2022) 105416, https://doi.org/10.1016/j.jobe.2022.105416.

[11] J. Hou, H. Li, N. Nord, G. Huang, Model predictive control for a university heat prosumer with data centre waste heat and thermal energy storage, *Energy* 267 (Mar. 2023) 126579, https://doi.org/10.1016/j.energy.2022.126579.

[12] L. Liu, Q. Zhang, Z. (John) Zhai, C. Yue, X. Ma, State-of-the-art on thermal energy storage technologies in data center, Energy Build. vol. 226, p. 110345, Nov. 2020, doi: 10.1016/j.enbuild.2020.110345.

[13] A. Vecchi, et al., Carnot Battery development: a review on system performance, applications and commercial state-of-the-art, *J. Storage Mater.* 55 (Nov. 2022) 105782, https://doi.org/10.1016/j.est.2022.105782.

[14] O. Dumont, Investigation of a heat pump reversible into an organic Rankine cycle and its application in the building sector, PhD Dissertation (2017).

[15] O. Dumont, G. F. Frate, A. Pillai, S. Lecompte, M. De paepe, and V. Lemort, "Carnot battery technology: a state-of-the-art review, J. Energy Storage 32 (2020) 101756, doi: 10.1016/j.est.2020.101756.

[16] G.F. Frate, L. Ferrari, U. Desideri, Multi-criteria investigation of a pumped thermal electricity storage (PTES) system with thermal integration and sensible heat storage, Energ. Conver. Manage. 208 (Mar. 2020) 112530, https://doi.org/10.1016/j.enconman.2020.112530.

[17] A. Laterre, O. Dumont, V. Lemort, F. Contino, Is waste heat recovery a promising avenue for the Carnot battery? Techno-economic optimisation of an electric booster-assisted Carnot battery integrated into different data centres, Energ. Conver. Manage. 301 (Feb. 2024) 118030, https://doi.org/10.1016/j.enconman.2023.118030.

[18] I. H. Bell, J. Wronski, S. Quoilin, V. Lemort, Pure and pseudo-pure fluid thermophysical property evaluation and the open-source thermophysical property library coolprop, Ind. Eng. Chem. Res. 53(6) (2014) Art. no. 6, doi: 10.1021/ie4033999.

[19] O. Dumont, S. Quoilin, V. Lemort, Experimental investigation of a reversible heat pump/organic Rankine cycle unit designed to be coupled with a passive house to get a net zero energy building, Int. J. Refrig 54 (Jun. 2015) 190–203, https://doi.org/10.1016/j.ijrefrig.2015.03.008.

[20] M. Bianchi, et al., Application and comparison of semi-empirical models for performance prediction of a kW-size reciprocating piston expander, Appl. Energy 249 (Sep. 2019) 143–156, https://doi.org/10.1016/j.apenergy.2019.04.070.
[21] O. Dumont, A. Charalampidis, V. Lemort, Experimental investigation of a thermally integrated carnot battery using a reversible heat pump/organic rankine cycle, International Refrigeration and Air Conditioning Conference, May 2021, [Online]. Available: https://docs.lib.purdue.edu/iracc/2085.
[22] R. Dickes, O. Dumont, R. Daccord, S. Quoilin, V. Lemort, Modelling of organic Rankine cycle power systems in off-design conditions: an experimentally-validated comparative study, Energy 123 (Mar. 2017) 710–727, https://doi.org/10.1016/j.energy.2017.01.130.
[23] V. Lemort, Contribution to the characterization of scroll machines in compressor and expander modes, University of Liège, 2008.
[24] M. Bianchi, et al., Replacement of R134a with low-GWP fluids in a kW-size reciprocating piston expander: performance prediction and design optimization, Energy 206 (2020) 118174, https://doi.org/10.1016/j.energy.2020.118174.
[25] N. Torricelli, L. Branchini, A. De Pascale, O. Dumont, V. Lemort, Optimal management of reversible heat pump/organic rankine cycle carnot batteries, J. Eng. Gas Turb. Power 145(4) (2023), doi: 10.1115/1.4055708.
[26] C. Poletto, O. Dumont, A. De Pascale, V. Lemort, S. Ottaviano, O. Thomé, Control strategy and performance of a small-size thermally integrated Carnot battery based on a Rankine cycle and combined with district heating, Energ. Conver. Manage. 302 (Feb. 2024) 118111, https://doi.org/10.1016/j.enconman.2024.118111.
[27] A.L. Nash, A. Badithela, N. Jain, Dynamic modeling of a sensible thermal energy storage tank with an immersed coil heat exchanger under three operation modes, *Appl. Energy* 195 (Jun. 2017) 877–889, https://doi.org/10.1016/j.apenergy.2017.03.092.
[28] S. Patankar, Numerical heat transfer and fluid flow. CRC Press, Boca Raton, 2018. doi: 10.1201/9781482234213.
[29] M. Wahlroos, M. Pärssinen, S. Rinne, S. Syri, J. Manner, Future views on waste heat utilization – case of data centers in Northern Europe, Renew. Sustain. Energy Rev. 82 (Feb. 2018) 1749–1764, https://doi.org/10.1016/j.rser.2017.10.058.
[30] C. Nadjahi, H. Louahlia, S. Masson, A review of thermal management and innovative cooling strategies for data center, Sustain. Comput. Informatics Syst. (2018), https://doi.org/10.1016/J.SUSCOM.2018.05.002.
[31] T. Sathesh, Y.-C. Shih, Optimized deep learning-based prediction model for chiller performance prediction, Data Knowl. Eng. 144 (Mar. 2023) 102120, https://doi.org/10.1016/j.datak.2022.102120.
[32] "JRC Photovoltaic Geographical Information System (PVGIS) - European Commission." Accessed: Dec. 17, 2021. [Online]. Available: https://re.jrc.ec.europa.eu/pvg_tools/it/#MR.
[33] A. Sohani, M.H. Shahverdian, H. Sayyaadi, D.A. Garcia, Impact of absolute and relative humidity on the performance of mono and poly crystalline silicon photovoltaics; applying artificial neural network, J. Clean. Prod. 276 (Dec. 2020) 123016, https://doi.org/10.1016/j.jclepro.2020.123016.
[34] "Most efficient solar panels 2023," Clean Energy Reviews. Accessed: Dec. 15, 2023. [Online]. Available: https://www.cleanenergyreviews.info/blog/most-efficient-solar-panels.
[35] G. Notton, C. Cristofari, M. Mattei, P. Poggi, Modelling of a double-glass photovoltaic module using finite differences, Appl. Therm. Eng. 25 (17) (Dec. 2005) 2854–2877, https://doi.org/10.1016/j.applthermaleng.2005.02.008.
[36] C. Arpagaus, F. Bless, M. Uhlmann, J. Schiffmann, S.S. Bertsch, High temperature heat pumps: market overview, state of the art, research status, refrigerants, and application potentials, Energy 152 (Jun. 2018) 985–1010, https://doi.org/10.1016/j.energy.2018.03.166.
[37] M. Bianchi, et al., Performance and total warming impact assessment of pure fluids and mixtures replacing HFCs in micro-ORC energy systems, Appl. Therm. Eng. 203 (2022).
[38] E. Hahne, Y. Chen, Numerical study of flow and heat transfer characteristics in hot water stores, Sol. Energy 64 (1) (Sep. 1998) 9–18, https://doi.org/10.1016/S0038-092X(98)00051-6.
[39] S. Lemmens, Cost engineering techniques and their applicability for cost estimation of organic rankine cycle systems, Energies 9(7) (2016), Art. no. 7, doi: 10.3390/en9070485.
[40] M. Shamoushaki, P. H. Niknam, L. Talluri, G. Manfrida, D. Fiaschi, Development of cost correlations for the economic assessment of power plant equipment, Energies 14(9) (2021) Art. no. 9, doi: 10.3390/en14092665.
[41] S. Lecompte, Performance evaluation of organic Rankine cycle architectures : application to waste heat valorisation," dissertation, Ghent University, 2016. Accessed: Mar. 09, 2023. [Online]. Available: http://hdl.handle.net/1854/LU-7223134.
[42] "Costi e tariffe del teleriscaldamento in Emilia Romagna." Accessed: Mar. 21, 2023. [Online]. Available: https://www.ilteleriscaldamento.eu/teleriscaldamento_emilia_romagna.htm.
[43] "GME - Gestore dei Mercati Energetici SpA." Accessed: Mar. 21, 2023. [Online]. Available: https://www.mercatoelettrico.org/It/Tools/Accessodati.aspx?ReturnUrl=%2fIt%2fdownload%2fDatiStorici.aspx.
[44] M.A. Ancona et al., Experimental and numerical investigation of a micro-ORC system for heat recovery from data centers, J. Phys.: Conf. Ser., vol. 2385, no. 1, p. 012122, Dec. 2022, doi: 10.1088/1742-6596/2385/1/012122.
[45] M. Bianchi, et al., Performance and operation of micro-ORC energy system using geothermal heat source, *Energy Procedia* 148 (Aug. 2018) 384–391, https://doi.org/10.1016/j.egypro.2018.08.099.
[46] M. Amir, et al., Energy storage technologies: an integrated survey of developments, global economical/environmental effects, optimal scheduling model, and sustainable adaption policies, *J. Storage Mater.* 72 (Nov. 2023) 108694, https://doi.org/10.1016/j.est.2023.108694.
[47] Y. Yang et al., An overview of application-oriented multifunctional large-scale stationary battery and hydrogen hybrid energy storage system, Energy Rev., p. 100068, Jan. 2024, doi: 10.1016/j.enrev.2024.100068.